ACS OMEGA

http://pubs.acs.org/journal/acsodf

Article

Anomalous Optical Properties of Citrazinic Acid under Extreme pH Conditions

Luigi Stagi, Stefania Mura, Luca Malfatti, Carlo Maria Carbonaro, Pier Carlo Ricci, Stefania Porcu, Francesco Secci, and Plinio Innocenzi*

Cite This: *ACS Omega* 2020, 5, 10958−10964

Read Online

ACCESS | Metrics & More | Article Recommendations | Supporting Information

ABSTRACT: Citrazinic acid (CZA) is a weakly fluorescent molecular compound whose optical properties are dependent on aggregation states and chemical environment. This molecule and its derivatives have been recently identified as the source of the intense blue emission of carbon dots obtained from citric acid with a nitrogen source, such as ammonia or urea. Citrazinic acid has a strong tendency to aggregate and form tautomers whose optical properties are largely unexplored. At extreme acidic and basic pH values, we have observed an "anomalous" optical response of citrazinic acid, attributed to the formation of aggregates from the tautomers. We have characterized the molecule, both at pH = 1 and 14, using UV−vis, NMR, steady-state, and time-resolved fluorescence spectroscopy. At extremely low pH values, the protonation causes luminescence quenching and the appearance of new emissions. On the contrary, high pH values are responsible for deprotonation and splitting of the excitation spectra.

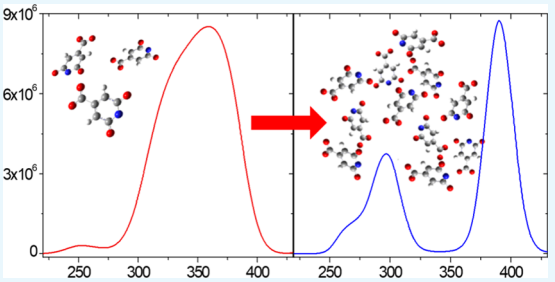

1. INTRODUCTION

Fluorescent molecular compounds are rapidly gaining the attention of researchers as new systems for implementing devices in applications ranging from light-emitting diodes (LEDs) (OLEDs, PLEDs) and organic−inorganic hybrid LEDs to active optical media for lasers or bioimaging systems.[1−5]

Carbon dots belong to this class of compounds. These systems have nanometric dimensions, excellent fluorescence properties, and an extraordinary simplicity of synthesis, based mostly on the thermal degradation of organic precursors that can take place both in dry conditions and in solutions (through reflux or hydro/solvothermal environment).[6] The excellent luminescent properties of carbon dots are generally governed by quantum and chemical-physical processes.[7] The former involves electronic recombination channels in the inner core region that displays a well-defined crystalline structure. In this context, the optical properties can be traced back to the variation in the size of the crystalline area and are based on the same principles of the more common quantum dots.[8] In the second case, the presence of fluorophores molecular species that are not involved in graphite condensation governs the emission of carbon dots. In this scenario, the identification of specific fluorophores is of great interest. However, very little is still known about the mechanisms providing the formation of these fluorophores and how a possible mutual interaction leads to a considerable quantum yield and the possibility of tuning the emission wavelengths.[9]

Citrazinic acid (CZA) is one of the molecular precursors behind the formation of highly fluorescent carbon dots. Investigating how the molecular aggregation of the fluorophores affects the optical properties of carbon dots could potentially inspire new methods of synthesis. Citrazinic acid strongly tends to form dimers at high concentrations. Although the mechanisms and the intrinsic characteristics of the aggregated forms are still far from being fully understood, it is speculated that the properties of carbon dots derive from aggregates of citrazinic acid and its derivatives. A change in the pH value may inhibit or promote the formation of aggregates and, correspondingly, influence the optical properties of aqueous solutions. In particular, fluorescence and absorption spectra are highly affected by protonation and deprotonation processes induced in acidic and basic environments, respectively.

Among the numerous fluorophores reported in the literature, citrazinic acid (CZA) has been identified as the main cause of the emission in the blue region by carbon dots, derived from the condensation of citric acid with a nitrogen source, such as ammonia or urea.[10]

Received: February 21, 2020
Accepted: March 27, 2020
Published: May 5, 2020

https://dx.doi.org/10.1021/acsomega.0c00775
ACS Omega 2020, 5, 10958−10964

Citrazinic acid consists of a ring of dihydroxy-pyridine with a substituting carboxylic acid group. A wide emission band in the visible range with a maximum around 440 nm is characteristic of CZA. It also has the tendency to tautomerism and formation of dimers.[11,12] The presence of dimers can substantially affect the optical properties of the molecule in solution. In our recent work,[11] we have shown that increasing the CZA concentration in aqueous solution gives rise to the formation of fluorescent dimers. The presence of dimers has been investigated by spectroscopic methods. In fact, dimers exhibit a distinct optical absorption and excitation spectrum and are associated with a red shift of photoluminescence compared to the monomer emission. CZA, at the same time, can form tautomers in acidic conditions. The stability of a tautomer depends on the pH values of the solution.[13] Correspondingly, we expect that the optical properties of CZA are strongly influenced by the protonation and deprotonation processes that occur at extreme pH values.

In this article, we have used a comprehensive spectroscopic characterization of CZA in strongly acidic and alkaline solutions aiming to highlight the role of proton addition or removal reactions on the molecular optical properties. We have observed an "anomalous" optical response, which is due to the formation of aggregates from the tautomers.

2. RESULTS AND DISCUSSION

Citrazinic acid presents an emission in the blue region of the visible spectrum, and different molecular forms, such as tautomers or aggregates, can arise in aqueous solution as a function of concentration and pH. To study the effect of pH on the CZA optical properties, we have used acidic and basic solutions of CZA at extreme pH values and we have combined several spectroscopic techniques and theoretical calculations.

Figure 1 shows the absorbance spectra of CZA in H_2O (black line) and H_2SO_4 (red curve). A strong absorption band

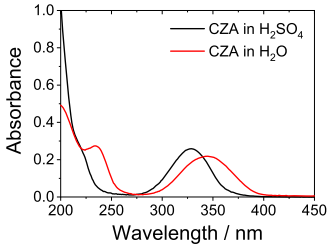

Figure 1. Absorbance spectra of CZA (10 mg L^{-1}) in H_2O and in H_2SO_4 (10%, v/v).

between 275 and 450 nm characterizes CZA. The $n\rightarrow\pi^*$ transition involving the excitation of lone pair in the pyridone moiety is at the origin of the absorption.[11] The maximum of this band has been reported to be strongly affected by the chemical environment.[11] In particular, in acidic conditions, we have observed a marked blue shift from 344 to 328 nm and a full width at half-maximum (FWHM) narrowing of 13 nm. In addition, the $\pi\rightarrow\pi^*$ band at 235 nm[11] in water is shifted down to about 218 nm to overlap the strong absorption at 200 nm ($\pi\rightarrow\pi^*$).

The shift toward lower wavelengths of the 235 nm band follows the lowering of the pH value (Figure 2). At pH 1, the hypsochromic shift stops at 214 nm, as shown by the deconvolutions of the high-energy structured band (Figure S1). Increasing the H_2SO_4 concentration does not induce any

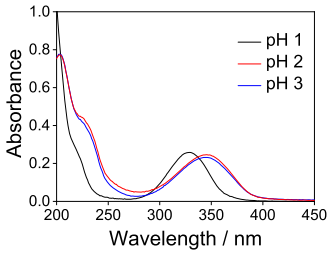

Figure 2. Absorbance spectra of CZA as a function of pH in H_2SO_4 solution (10 mg L^{-1}).

further shift but a gradual increase of the absorbance (see Figure S2).

The study of emission and excitation properties can provide new clues about what happens in a strongly acidic solution.

Figure 3 shows the three-dimensional (3D) fluorescence spectra [excitation (y)−emission (x)−intensity (z)] of CZA in

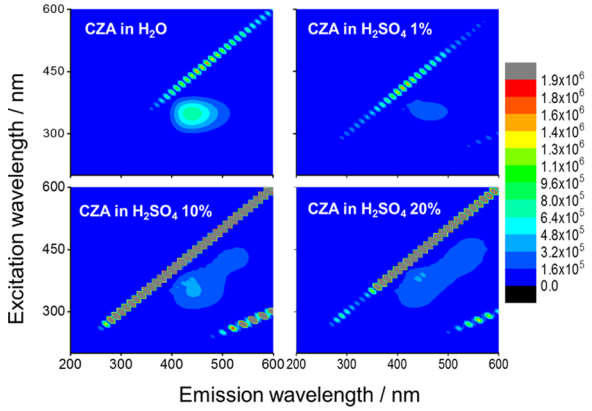

Figure 3. 3D fluorescence spectra (excitation−emission−intensity) of CZA (10 mg L^{-1}) in water and in H_2SO_4 solutions (1, 10, and 20%, v/v).

water and in acidic solutions. CZA in water presents a symmetric pattern in excitation with the intensity maximum at λ_{ex} = 344 nm and λ_{em} = 440 nm. The excitation maximum is in good accordance with the absorption spectrum of Figure 1. Under excitation at 344 nm, the CZA displays a broad-band emission ascribed to a single monomeric chemical species.[11] In acidic conditions, the three-dimensional (3D) pattern intensity undergoes a considerable change and, correspondingly, a new band at lower wavelengths appears. At 1% (v/v) of H_2SO_4 concentration, CZA intensity is quenched of about 1 order of magnitude and keeps lowering at higher concentrations.

Figure 4 shows the excitation (PLE) and emission (PL) spectra of CZA at 10% (v/v) H_2SO_4 concentration. By monitoring the emission at 440 nm, an excitation band with maximum at about 348 nm is observed. This excitation curve well reproduces the absorption spectrum for $n\rightarrow\pi^*$ transition and is attributed to the excitation of CZA monomer in aqueous solution.[11] The green band at 530 nm displays a two-component excitation spectrum with two maxima at 345 and 430 nm. Still, the former corresponds to the excitation of CZA in pure water. The second excitation band represents a new feature of CZA in an acidic environment.

At a high acid concentration, CZA is in a full protonated configuration[14] (Scheme 1). In principle, the presence of a protonated form can promote a dimerization process with

https://dx.doi.org/10.1021/acsomega.0c00775
ACS Omega 2020, 5, 10958−10964

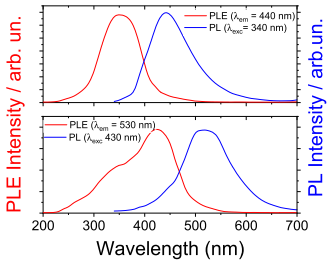

Figure 4. Excitation and emission spectra of CZA in H_2SO_4 (10%) at 10 mg L^{-1}.

Scheme 1. Effect of Basic and Acidic Solutions on Monomer Molecular Structures

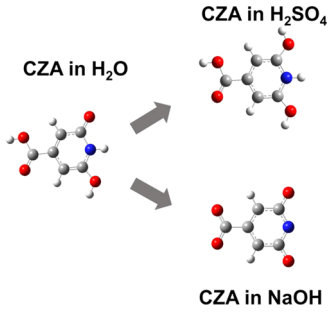

consequent formation of new aggregates that show new optical properties. These aggregates, present in a small amount, can be identified by monitoring their weak emission at larger wavelengths.

The main absorption at 328 nm in H_2SO_4 is due to the protonated monomeric configuration of CZA. The hypsochromic shift with respect to the aqueous solution is attributable to the adjustment of electronic distribution after the protonation process. This also affects the $\pi \rightarrow \pi^*$ band at higher energy, as shown in Figure 1.

After having investigated the optical properties of CZA in strong acid solutions, we have moved to the other extreme, very high basic conditions. Figure 5 shows the absorbance

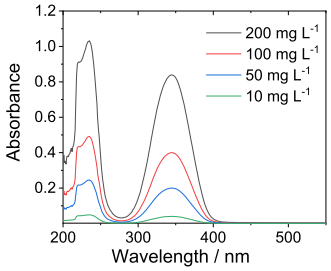

Figure 5. Absorbance spectrum of CZA in NaOH (pH 14) at concentrations of 10, 50, 100, and 200 mg L^{-1}.

spectrum of CZA in aqueous solutions of NaOH at pH 14. At 10 mg L^{-1}, CZA exhibits a very different and apparently anomalous optical absorption spectra. Two intense bands with maxima at 344 and 234 nm are in fact detected. The former has the same spectral characteristics of bandwidth and maximum position as the $n \rightarrow \pi^*$ transition in water. The band at lower wavelengths appears in water as well. However, under basic conditions, the absorption transition at around 200 nm, which has the highest attenuation value in water, is inhibited. No significant spectral differences (maxima positions and bands ratios) are appreciable as the concentration of CZA in solution increases, except for the overall increase in light attenuation. Moreover, the absorbance at 344 nm in NaOH is about 4 times the one measured in water, at the same concentration.

The 3D fluorescence maps, shown in Figure 6, provide further information on the effects of CZA concentration in

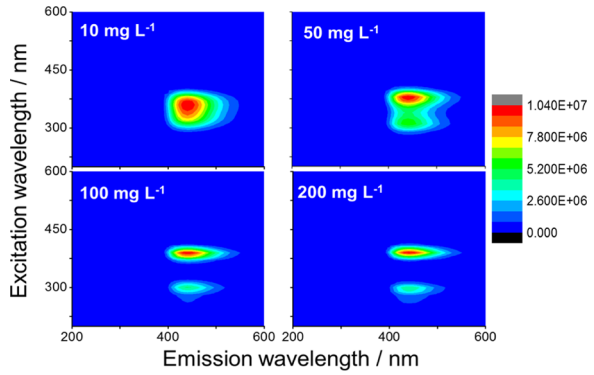

Figure 6. 3D fluorescence maps (emission−excitation intensity) of CZA in NaOH solutions at pH 14 as a function of concentration (10, 50, 100, 200 mg L^{-1}).

strong alkaline solutions. Starting at the concentration of 10 mg L^{-1}, the 3D pattern shows a band consisting of two overlapped components. By increasing the concentration of CZA, the two components tend to split into two well-defined bands. At 50 mg L^{-1}, the splitting of the two bands becomes appreciable. Finally, the two components are completely split at the concentration of 100 mg L^{-1}. Only a slight shift is appreciable at 200 mg L^{-1}. The general trend can be followed more accurately by extracting the excitation spectra (PLE), as shown in Figure 7. The PLE spectra were acquired by monitoring the emission band maximum at 440 nm, being independent of concentration variations.

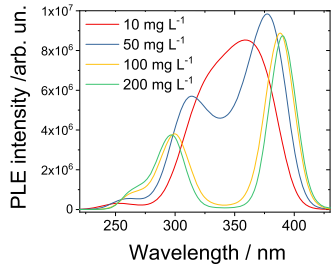

Figure 7. Excitation spectra of CZA in NaOH (pH 14) as a function of concentration (10, 50, 100, 200 mg L^{-1}).

The spectrum at 10 mg L^{-1} shows an excitation band with a maximum at 358 nm, which can be deconvolved into two components at 3.40 and 3.78 eV (Figure S3). In addition, there is a weak band at about 4.96 eV (250 nm), which is responsible for the high-energy contribution of the absorption spectrum ($\pi \rightarrow \pi^*$). At 50 mg L^{-1}, the two excitation bands $n \rightarrow \pi^*$ separate toward opposite directions at 377 nm (3.29 eV) and 320 nm (3.88 eV). At higher concentrations, the two bands are at 390 nm (3.18 eV) and 297 nm (4.18 eV). The excitation band at a higher energy shifts to 270 nm (4.59 eV).

The study of the photoluminescence kinetic may provide further information for the interpretation of the collected

https://dx.doi.org/10.1021/acsomega.0c00775
ACS Omega 2020, 5, 10958−10964

steady-state data. Time-resolved photoluminescence (TR-PL) measurements have been carried out on CZA at extreme pH conditions. Figure 8 shows the PL decay profile of CZA in

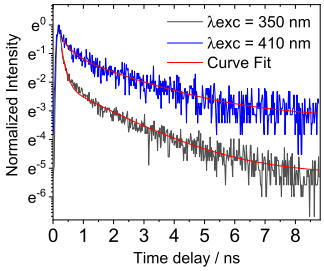

Figure 8. Time-resolved spectra of CZA in H_2SO_4 (pH 1) at excitation wavelengths of 350 nm (black curve) and 410 nm (blue curve).

acidic conditions. According to the excitation spectra, which have revealed the presence of two components, the sample has been irradiated at 350 and 410 nm, to study the emission at 440 and 530 nm, respectively. The component at 440 nm presents a double-exponential decay, with an average time of $\tau^* = 0.5$ ns. The component at 530 nm can be also fitted with two exponentials and an average lifetime of $\tau^* = 2$ ns. The trend of luminescence kinetics suggests the formation of CZA dimers by protonation. In general, these aggregates are weakly fluorescent as the nonradiative recombination is highly favored.[2,11]

CZA at pH 14 has been excited at two different wavelengths as displayed by the excitation spectra (Figure 7). $\lambda_{exc} = 300$ and 380 nm have been considered as a good compromise for the two excitation channels of CZA at different concentrations. The corresponding PL decay in the scale of 50 ns is reported in Figure 9. Under both excitation wavelengths, the photo-

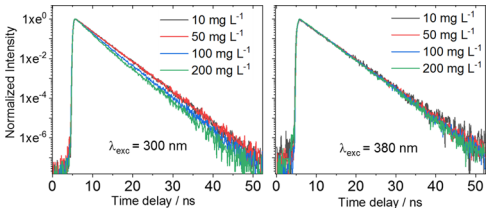

Figure 9. Time-resolved spectra of CZA in NaOH (pH 14) as a function of concentration (10, 50, 100, 200 mg L^{-1}). (a) Excitation at 300 nm and (b) 380 nm.

luminescence decays through a single-exponential law $I = A \exp(-t/\tau)$. Under $\lambda_{exc} = 300$ nm, the CZA at the concentration of 10 mg L^{-1} displays a decay lifetime of $\tau = 6.5$ ns, in good accordance with CZA in pure water.[11] As the CZA concentration increases, we assist to a slight decrease of lifetime value down to 5.5 ns at the highest concentration (200 mg L^{-1}). This can be attributed to a weak interaction of neighboring molecules at the increase of concentration, contributing to enhance the nonradiative component ($\tau^{-1} = \tau_{radiative}{}^{-1} + \tau_{non\text{-}radiative}{}^{-1}$). Under the excitation at 380 nm, CZA does not show a significant difference as a function of concentration, retaining a lifetime of 6.5 ns. Time-resolved spectra confirm that CZA in alkaline conditions show a kinetics of PL decay attributable to a monomeric form.

NMR measurements in basic conditions have provided experimental evidence of deprotonation of carboxylic groups in CZA (NMR data are reported in Figure S4).

As shown in the experimental results, absorption spectra significantly change as a function of pH value. It turns out that the absorption is dependent on the acidity or alkalinity index of the solution. In particular, it is observed that the acidic environment promotes a blue shift of the 300−350 absorption band and the base affects the bands in the range of 200−270 nm.

Computational analysis of the molecule in different environments can help in the interpretation of the experimental data. To simulate the CZA molecule under different pH conditions, two possible structures have been hypothesized and optimized in their geometry (Figure 10). The resulting structures have been utilized for the calculation of UV−vis spectra by time dependent-density functional theory (TD-DFT). More precisely, a fully protonated CZA structure has been assumed as a model for the study at low pH values. In contrast, fully deprotonated CZA has been supposed for simulations in alkaline environments. The latter is also supported by NMR measurements.

Figure 10a shows the theoretical UV−vis spectra in the range of 150−550 nm. As already reported in our previous work,[11] the adopted computational level very well reproduces the absorption features of CZA molecule. A molecular orbital attribution of the main transition bands is reported in Figure 10b. When fully protonated, CZA_{prot} displays a strong blue shift of 46 nm. The strongest absorption lines at 196 nm in CZA are almost unchanged with the protonation of pyridine moiety, while the weak transition at around 222 nm undergoes a blue shift of 8 nm and a weakening of oscillator strength. Albeit with some differences, the theoretical UV−vis spectra are in good accordance with the experimental data, allowing for inferring that the absorption characteristics of CZA in sulfuric acid are dominated by the protonated configuration of the molecule. CZA_{deprot} has been selected as the best guess for high-pH solutions. $n \rightarrow \pi^*$ appears almost unmodified as the protons are removed, confirming the experimental trend (Figure 5). In the absence of hydrogen terminations, the transitions at high energies appear at around 250 nm. This shift reproduces the corresponding experimental UV−vis spectra. Moreover, it is worth underlining the growth of $n \rightarrow \pi^*/\pi \rightarrow \pi^*$ ratio after deprotonation, as experimentally measured.

Unlike in acidic conditions, where photoluminescence shows significant changes, CZA in NaOH does not show any variation in the emission spectrum, exhibiting the characteristic emission of the monomer. If the corresponding absorption can be correlated to the deprotonation of carboxyl and hydroxyl groups, the excitation spectra show a unique trend as a function of concentration. The splitting recorded in excitation is a typical signature of dimer formation.[15,16] According to the excitonic theory of Kasha,[17] a molecular system can undergo a strong and narrow red shift as a result of the formation of J-dimers, type of aggregated manifesting a coplanar alignment. H-dimers, in stacking configuration, typically show a blue shift and a corresponding quenching of fluorescence. Both the effects are observable in absorbance and become more marked as the monomers come closer, that is, as a function of concentration. A third possible configuration is allowed. Oblique aggregates, i.e., intermediate configurations between H- and J-, exhibit high- and low-energy transitions allowed, providing a measurable splitting in absorption (Davydov

https://dx.doi.org/10.1021/acsomega.0c00775
ACS Omega 2020, 5, 10958−10964

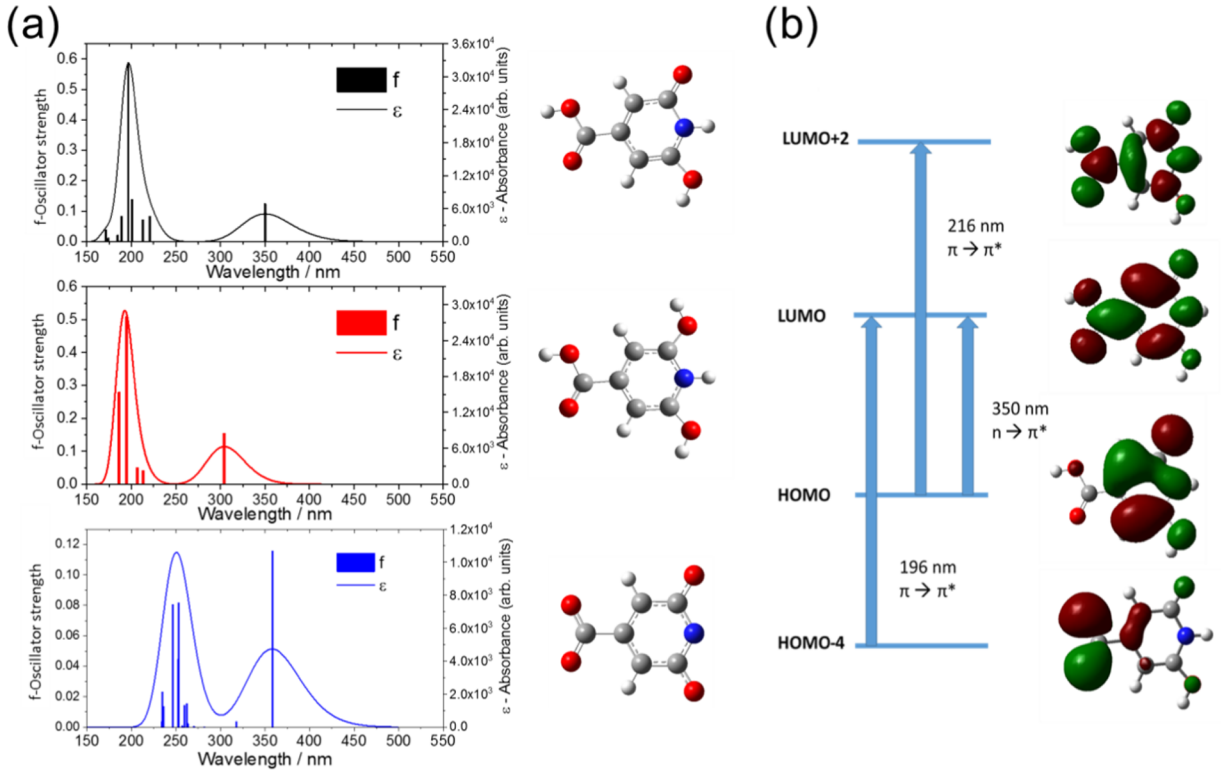

Figure 10. (a) Calculated UV−vis spectra of CZA molecules, protonated CZA (CZA_{prot}) and deprotonated CZA (CZA_{deprot}). (b) Molecular orbitals of CZA. The molecular orbitals were plotted taking into account the transitions with higher oscillator strength for each absorption band.

splitting).[15] In the case of CZA in NaOH, the splitting is only appreciable in the excitation spectra, whereas the absorption band at 344 nm keeps unaffected by pH increase. In light of this, the recorded photoluminescence as a function of excitation wavelength represents a measure of the recombination transitions. According to experimental results, the fluorescent recombination at 440 nm corresponding to the absorption at 344 nm becomes forbidden as dimers form. Correspondingly, only the absorptions at higher (λ > 340 nm) and lower (λ < 340 nm) wavelengths cause an allowed luminescent transition.

Still, the nature of dimers has to be figured out. In pyridine systems, the formation of dimers is strongly favored and is mainly mediated by the presence of protons at the hydroxyl groups or at the nitrogen groups in the form of amines.[18] In these cases, the established dynamic equilibrium of proton exchange favors the stability of the aggregate. In our case, the high pH promotes the deprotonation of the molecule and, correspondingly, a salt is formed. It has been reported that the presence of alkali cations favors the formation of dimers.[19] In particular, the binding of alkali ions can promote the dimerization of cluster and a consequent structural change. The bridging effect of cations depends on the size and, in turn, influences the dimerization degree. Therefore, we can assume that the presence of salt determines a weak interaction among molecular units in solution, originating the new feature in excitation.

3. CONCLUSIONS

The investigation of CZA in solutions with acidic pH (∼1) and basic pH (∼14) revealed substantial differences from the optical properties measurable in pure water.

In sulfuric acid, CZA undergoes a significant luminescence quenching with the consequent formation of new molecular species as evidenced by excitation spectra. The corresponding absorption spectrum shows a strong hypsochromic shift that is attributed to the protonation of the molecule. Computational calculations have accurately reproduced the experimental trend. The corresponding time-resolved measures show a reduction of lifetime compared to the monomer, in accordance with the formation of weakly fluorescent aggregates.

At pH 14, citrazinic acid maintains the emission spectrum of its monomeric form. The absorption spectrum shows no change in the transition at lower energy ($n \rightarrow \pi^*$) and a red shift of the higher-energy $\pi \rightarrow \pi^*$ absorption. This effect has been reproduced by computational calculations by tentatively imposing the formation of a deprotonated configuration. In this scenario, the increase in CZA concentration has an impact on excitation spectra showing a maximum splitting of about 90 nm in the analyzed concentration range. This effect can be interpreted in the framework of the formation of aggregates, which according to Davydov's theory are identified as obliquely favored aggregate monomers by the presence of alkali cations even if the mechanism that leaves the emission spectrum and low-energy absorption unaltered is not fully revealed by spectroscopic investigation.

4. EXPERIMENTAL AND THEORETICAL METHODS

Citrazinic acid (purity 97%, Sigma-Aldrich) and water (Milli-Q) were used as received without further purification. CZA, in powder form, was dissolved in aqueous solutions of H_2SO_4 at progressive decreasing of pH down to 1. The optical properties of CZA at 1, 10, and 20% (v/v) of acid concentration were analyzed. Similarly, the powder was dissolved in basic solution

https://dx.doi.org/10.1021/acsomega.0c00775
ACS Omega 2020, 5, 10958−10964

of NaOH at pH 14. The corresponding solutions were finally neutralized to verify the reproducibility of the measurements.

4.1. Experimental Methods. UV−vis measurements of CZA solubilized in water were performed using a Nicolet Evolution 300 spectrophotometer from 200 to 600 nm, employing quartz cuvettes of 1 and 0.1 cm light-path.

Steady-state optical response of the CZA solutions was investigated by 3D fluorescence mapping [excitation (y)−emission (x)−intensity (z)] using a Horiba Jobin Yvon FluoroMax-3 spectrofluorometer equipped with a 450 W xenon lamp as the excitation source. The maps were collected in the excitation/emission range of 200−700 nm, a 1 nm slit for excitation and emission.

TR-PL measurements were recorded by exciting the samples with 200 fs long pulses delivered by an optical parametric amplifier (Light Conversion TOPAS-C) pumped by a regenerative Ti:sapphire amplifier (Coherent Libra-HE). The repetition frequency was 1 kHz, and the PL signal was recovered by a streak camera (Hamamatsu C10910) equipped with a grating spectrometer (Princeton Instruments Acton SpectraPro SP-2300). All of the measurements were collected in the front-face configuration to reduce inner filter effects. Proper optical filters were applied to remove the reflected contribution of the excitation light.

^{1}H NMR spectra were recorded on a 500 MHz Varian spectrometer at 25 °C using dimethyl sulfoxide (DMSO) (2.50 ppm) as a solvent. ^{1}H NMR measurements were carried out using 4 mg (0.026 mmol) of CZA dissolved in 1 mL of DMSO-d_6 after sonication for 10 min at room temperature.

4.2. Computational Methods. All of the calculations were carried out using Gaussian 16 code.[20] The energy calculations of the optimized structures were performed within density functional theory (DFT) with Becke's three parameters and the Lee−Yang−Parr's nonlocal correlation functional (B3LYP).[21−23] The basis sets for C, N, O, and H were 6-311++G(d,p), while the electronic excitation energies were calculated on the basis of the TD-DFT method. The analysis of frequencies confirms that optimized structures are at a minimum of potential surface, and no imaginary frequencies were obtained. The calculations were performed using both water and vacuum as the medium. GaussView 6 was used to interpret the computed data.[24]

■ ASSOCIATED CONTENT

Supporting Information

The Supporting Information is available free of charge at https://pubs.acs.org/doi/10.1021/acsomega.0c00775.

Curve fit of absorbance and excitation spectra; absorbance at a high concentration of sulfuric acid, and NMR (PDF)

■ AUTHOR INFORMATION

Corresponding Author

Plinio Innocenzi − *Department of Chemistry and Pharmacy, Laboratory of Materials Science and Nanotechnology, CR-INSTM, University of Sassari, 07100 Sassari, Italy;* orcid.org/0000-0003-2300-4680; Email: plinio@uniss.it

Authors

Luigi Stagi − *Department of Chemistry and Pharmacy, Laboratory of Materials Science and Nanotechnology, CR-INSTM, University of Sassari, 07100 Sassari, Italy;* orcid.org/0000-0002-7238-8425

Stefania Mura − *Department of Chemistry and Pharmacy, Laboratory of Materials Science and Nanotechnology, CR-INSTM, University of Sassari, 07100 Sassari, Italy*

Luca Malfatti − *Department of Chemistry and Pharmacy, Laboratory of Materials Science and Nanotechnology, CR-INSTM, University of Sassari, 07100 Sassari, Italy;* orcid.org/0000-0001-6901-8506

Carlo Maria Carbonaro − *Department of Physics, University of Cagliari, 09042 Monserrato, Italy;* orcid.org/0000-0001-6353-6409

Pier Carlo Ricci − *Department of Physics, University of Cagliari, 09042 Monserrato, Italy;* orcid.org/0000-0001-6191-4613

Stefania Porcu − *Department of Physics, University of Cagliari, 09042 Monserrato, Italy*

Francesco Secci − *Department of Chemical and Geological Sciences and INSTM, University of Cagliari, 09042 Monserrato, Italy;* orcid.org/0000-0003-0443-2890

Complete contact information is available at: https://pubs.acs.org/10.1021/acsomega.0c00775

Author Contributions

The manuscript was written through contributions of all authors. All authors have given approval to the final version of the manuscript.

Notes

The authors declare no competing financial interest.

■ ACKNOWLEDGMENTS

Italian Ministry of Education, University and Research (MIUR) is acknowledged for funding through the project PRIN 2017 no. 2017W75RAE. University of Sassari is also acknowledged for funding through "fondo di ateneo per la ricerca 2019."

■ REFERENCES

(1) Stagi, L.; Chiriu, D.; Carbonaro, C. M.; Corpino, R.; Ricci, P. C. Structural and optical properties of carbon nitride polymorphs. *Diamond Relat. Mater.* **2016**, *68*, 84−92.

(2) Luridiana, A.; Pretta, G.; Chiriu, D.; Carbonaro, C. M.; Corpino, R.; Secci, F.; Frongia, A.; Stagi, L.; Ricci, P. C. A facile strategy for new organic white LED hybrid devices: design, features and engineering. *RSC Adv.* **2016**, *6*, 22111−22120.

(3) Stagi, L.; Chiriu, D.; Scholz, M.; Carbonaro, C. M.; Corpino, C.; Porcheddu, A.; Rajamaki, S.; Cappellini, G.; Cardia, R.; Ricci, P. C. Vibrational and optical characterization of s-triazine derivatives. *Spectrochim. Acta, Part A* **2017**, *183*, 348−355.

(4) Burn, P. L.; Lo, S. C.; Samuel, I. D. W. The development of light-emitting dendrimers for displays. *Adv. Mater.* **2007**, *19*, 1675−1688.

(5) Stagi, L.; Chiriu, D.; Ardu, A.; Cannas, C.; Carbonaro, C. M.; Ricci, P. C. Luminescence enhancement by energy transfer in melamine-Y_2O_3:Tb^{3+} nanohybrids. *J. Appl. Phys.* **2015**, *118*, 125502−125507.

(6) Ludmerczki, R.; Mura, S.; Carbonaro, C. M.; Mandity, I. M.; Carraro, M.; Senes, N.; Garroni, S.; Granozzi, G.; Calvillo, L.; Marras, S.; Malfatti, L.; Innocenzi, P. Carbon Dots from Citric Acid and its Intermediates Formed by Thermal Decomposition. *Chem. - Eur. J.* **2019**, *25*, 11963−11974.

(7) Reckmeier, C. J.; Schneider, J.; Xiong, Y.; Häusler, J.; Kasák, P.; Schnick, W.; Rogach, A. L. Aggregated Molecular Fluorophores in the ammonothermal Synthesis of Carbon Dots. *Chem. Mater.* **2017**, *29*, 10352−10361.

(8) Suzuki, K.; Malfatti, L.; Takahashi, M.; Carboni, D.; Messina, F.; Tokudome, Y.; Takemoto, M.; Innocenzi, P. Design of Carbon Dots Photoluminescence through Organo-Functional Silane Grafting for Solid-State Emitting Devices. *Sci. Rep.* **2017**, *7*, No. 5469.
(9) Zhu, S.; Zhao, X.; Song, Y.; Lu, S.; Yang, B. Beyond Bottom-up Carbon Nanodots: Citric-Acid Derived Organic Molecules. *Nano Today* **2016**, *11*, 128−132.
(10) Kasprzyk, W.; Świergosz, T.; Bednarz, S.; Walas, K.; Bashmakova, N. V.; Bogdała, D. Luminescence phenomena of carbon dots derived from citric acid and urea − a molecular insight. *Nanoscale* **2018**, *10*, 13889−13894.
(11) Mura, S.; Stagi, L.; Malfatti, L.; Carbonaro, C. M.; Ludmerczki, R.; Innocenzi, P. Modulating the Optical Properties of Citrazinic Acid through the Monomer-to-Dimer Transformation. *J. Phys. Chem. A* **2020**, *124*, 197−203.
(12) Bunting, J. W.; Kanter, J. P. Acidity and tautomerism of β-keto esters and amides in aqueous solution. *J. Am. Chem. Soc.* **1993**, *115*, 11705−11715.
(13) Rauf, M. A.; Hisaindee, S.; Saleh, N. Spectroscopic studies of keto−enol tautomeric equilibrium of azo dyes. *RSC Adv.* **2015**, *5*, 18097−18110.
(14) Sarkar, S.; Chowdhury, J.; Dutta, S.; Pal, T. A pH dependent Raman and surface enhanced Raman spectroscopic studies of citrazinic acid aided by theoretical calculations. *Spectrochim. Acta, Part A* **2016**, *169*, 108−115.
(15) Fothergill, J. W.; Hernandez, A. C.; Knowlton, W. B.; Yurke, B.; Li, L. Ab-Initio Studies of Exciton Interactions of Cy5 Dyes. *J. Phys. Chem. A* **2018**, *122*, 8989−8997.
(16) Yoon, M.; Miyamoto, Y.; Scheffler, M. Enhanced dipole moments in photo-excited TTF−TCNQ dimers. *New J. Phys.* **2011**, *13*, No. 073039.
(17) Kasha, M. Energy Transfer Mechanisms and the Molecular Exciton Model for Molecular Aggregates. *Radiat. Res.* **1963**, *20*, 55−70.
(18) Ottiger, P.; Köppel, H.; Leutwyler, S. Excitonic splittings in molecular dimers: why static ab initio calculations cannot match them. *Chem. Sci.* **2015**, *6*, 6059−6068.
(19) Chakraborty, P.; Baksi, A.; Mudedla, S. K.; Nag, A.; Paramasivam, G.; Subramanian, V.; Pradeep, T. Understanding Proton Capture and Cation-Induced Dimerization of $[Ag_{29}(BDT)_{12}]^{3-}$ Clusters by Ion Mobility Mass Spectrometry. *Phys. Chem. Chem. Phys.* **2018**, *20*, 7593−7603.
(20) Frisch, M. J.; Trucks, G. W.; Schlegel, H. B.; Scuseria, G. E.; Robb, M. A.; Cheeseman, J. R.; Scalmani, G.; Barone, V.; Petersson, G. A.; Nakatsuji, H.; Li, X.; Caricato, M.; Marenich, A. V.; Bloino, J.; Janesko, B. G.; Gomperts, R.; Mennucci, B.; Hratchian, H. P.; Ortiz, J. V.; Izmaylov, A. F.; Sonnenberg, J. L.; Williams-Young, D.; Ding, F.; Lipparini, F.; Egidi, F.; Goings, J.; Peng, B.; Petrone, A.; Henderson, T.; Ranasinghe, D.; Zakrzewski, V. G.; Gao, J.; Rega, N.; Zheng, G.; Liang, W.; Hada, M.; Ehara, M.; Toyota, K.; Fukuda, R.; Hasegawa, J.; Ishida, M.; Nakajima, T.; Honda, Y.; Kitao, O.; Nakai, H.; Vreven, T.; Throssell, K.; Montgomery, J. A.; Peralta, J. E.; Ogliaro, F.; Bearpark, M. J.; Heyd, J. J.; Brothers, E. N.; Kudin, K. N.; Staroverov, V. N.; Keith, T. A.; Kobayashi, R.; Normand, J.; Raghavachari, K.; Rendell, A. P.; Burant, J. C.; Iyengar, S. S.; Tomasi, J.; Cossi, M.; Millam, J. M.; Klene, M.; Adamo, C.; Cammi, R.; Ochterski, J. W.; Martin, R. L.; Morokuma, K.; Farkas, O.; Foresman, J. B.; Fox, D. J. *Gaussian 16*, Revision C.01; Gaussian, Inc.: Wallingford, CT, 2016.
(21) Jiang, J.; Ou-yang, L.; Zhu, L.; Zheng, A.; Zou, J.; Yi, X.; Tang, H. Dependence of electronic structure of g-C3N4 on the layer number of its nanosheets: A study by Raman spectroscopy coupled with first-principles calculations. *Carbon* **2014**, *80*, 213−221.
(22) Becke, A. D. Density-functional thermochemistry. III. The role of exact exchange. *J. Chem. Phys.* **1993**, *98*, 5648−5652.
(23) Lee, C.; Yang, W.; Parr, R. G. Development of the Colle-Salvetti correlation-energy formula into a functional of the electron density. *Phys. Rev. B* **1988**, *37*, 785−789.
(24) Dennington, R.; Keith, T. A.; Millam, J. M.. *GaussView*, Version 6, Semichem Inc.: Shawnee Mission, KS, 2016.

https://dx.doi.org/10.1021/acsomega.0c00775
ACS Omega 2020, 5, 10958−10964